Agricultural and Forest Meteorology 247 (2017) 520–532

Contents lists available at ScienceDirect

Agricultural and Forest Meteorology

journal homepage: www.elsevier.com/locate/agrformet

Research Paper

Patterns and controls of carbon dioxide and water vapor fluxes in a dry forest of central Argentina

Alfredo G. García[a], Carlos M. Di Bella[a,b], Javier Houspanossian[c], Patricio N. Magliano[c], Esteban G. Jobbágy[c], Gabriela Posse[a], Roberto J. Fernández[d], Marcelo D. Nosetto[c,e,*]

[a] Instituto de Clima y Agua, Instituto Nacional de Tecnología Agropecuaria (CIRN-INTA Castelar), Hurlingham, Buenos Aires, Argentina
[b] Departamento de Métodos Cuantitativos, Universidad de Buenos Aires, Facultad de Agronomía, Buenos Aires, Argentina
[c] Grupo de Estudios Ambientales (GEA), IMASL, CONICET & UNSL, San Luis, Argentina
[d] Instituto de investigación Fisiológicas y Ecológicas Vinculado a la Agricultura, IFEVA, CONICET & Univ. Buenos Aires, Argentina
[e] Cátedra de Climatología, Facultad de Ciencias Agropecuarias, Universidad Nacional de Entre Ríos,, Entre Ríos, Argentina

ARTICLE INFO

Keywords:
Eddy covariance
Deforestation
Chaco
Net ecosystem exchange
Carbon balance

ABSTRACT

Covering 16% of global land surface, dry forests play a key role in the global carbon budget. The Southern Hemisphere still preserves a high proportion of its native dry forest cover, but deforestation rates have increased dramatically in the last decades. In this paper, we quantified for the first time the magnitude and temporal variability of carbon dioxide and water vapor fluxes and their environmental controls based on eddy covariance measurements in a dry forest site of central Argentina. Continuous measurements of CO_2 and water vapor exchanges spanning a 15-month period (Dec. 2009 – March 2011) showed that the studied dry forest was a net sink of carbon, with an overall integrated net ecosystem exchange (NEE) of -172 g C m^{-2} (-132.8 g C m^{-2} for year 2010). The cool dry season (May–Sept.) accounted for a quarter of the total annual NEE of year 2010 with low but steady CO_2 uptake rates (1 g C m^{-2} d^{-1} on average) that were more strongly associated with temperature than with soil moisture. By contrast, in the warm wet season (Oct.–April), almost three times greater CO_2 uptake rates (2.7 g C m^{-2} d^{-1} on average) resulted from a highly pulsed behavior in which CO_2 uptake showed sharp increases followed by rapid declines after rainfall events. Cumulative evapotranspiration (ET) during the whole study (595 mm) accounted for most of the rainfall inputs (674 mm), with daily water vapor fluxes during the wet season being four times greater compared to those observed during the dry season (1.7 mm d^{-1} vs. 0.45 mm d^{-1}). Modeling of the partition of all evaporative water losses suggested that transpiration was the dominant vapor flux (67% of ET), followed by interception (20%) and soil evaporation (13%). The influence of air temperature on half-hourly CO_2 fluxes was notably different for the dry and wet seasons. In the 11–34 °C air temperature range, CO_2 uptake rates were higher in the warm wet rather than the cool dry season, yet this difference narrowed with temperatures > 26 °C. The dry forest became a net CO_2 source at 40 °C. Our study provides new insights about the functioning of dry forests and the likely response of their CO_2 and water vapor exchange with the atmosphere under future climate and land use/cover changes.

1. Introduction

Dry forests cover ~16% of global land surface (Olson et al., 2001) and because of land-use changes, fires and climate regime shifts (Fischer et al., 2012; Houspanossian et al., 2016; Smith et al., 2000) are one of the most threatened ecosystems worldwide (Hoekstra et al., 2005). The South American dry forests of Chaco and Espinal, extending over 1.4 million km^2, are no exception to these trends. This region encompass the second forest extension in South America after Amazonia, still preserving most of their area (~70%) covered by native vegetation (Houspanossian et al., 2016). However, deforestation rates have sped up dramatically in the last two decades, achieving record rates worldwide (Hansen et al., 2013; Vallejos et al., 2015). The region is also experiencing noticeable climatic changes which interact with technological and socioeconomic factors to drive land use changes (Zak et al., 2008). The understanding of carbon dioxide and water vapor fluxes patterns and their controls over such vast forests, is particularly important given the size of the carbon stocks that they host and the significance of their water fluxes shaping landscape hydrology and continental climate (Marchesini et al., 2016; Saulo et al., 2007).

* Corresponding author at: Grupo de Estudios Ambientales, Instituto de Matemática Aplicada San Luis, Italia 1556 – Ciudad de San Luis (5700), Argentina.
E-mail addresses: marcelo.nosetto@gmail.com, mnosetto@unsl.edu.ar (M.D. Nosetto).

http://dx.doi.org/10.1016/j.agrformet.2017.08.015
Received 19 February 2017; Received in revised form 10 August 2017; Accepted 14 August 2017

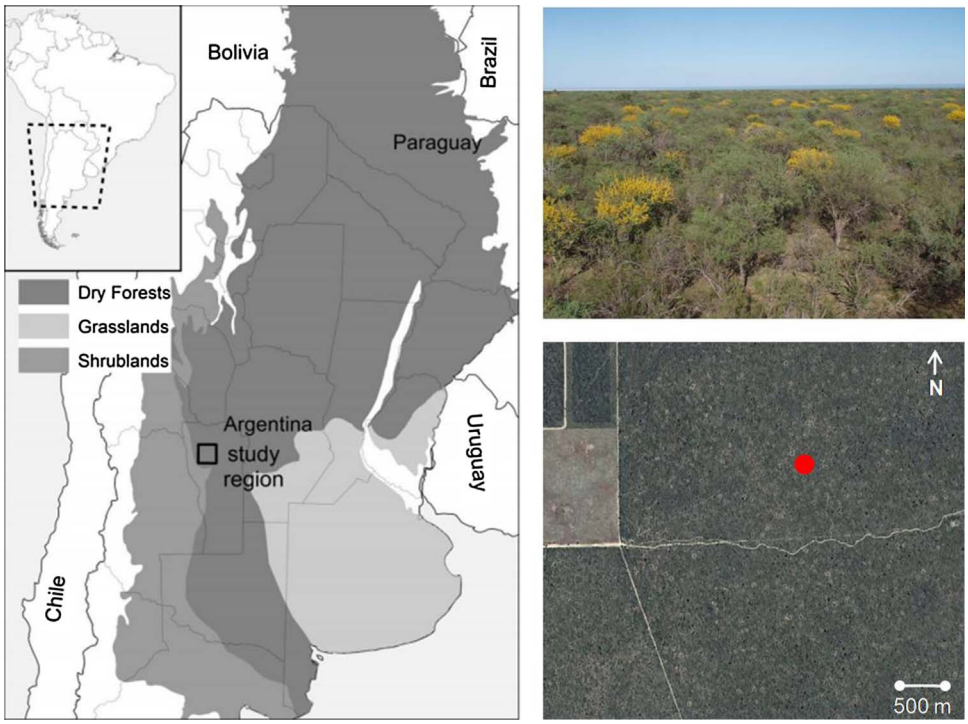

Fig. 1. Location of the study region in the dry forests of central Argentina. The original extension of the dominant biomes of the region is indicated on the map on the left. On the right, a Google Earth image (bottom) and a photograph taken at the field (top) show a typical dry forest stand. The red dot on the Google Earth image indicates the location of the measurement tower. (For interpretation of the references to colour in this figure legend, the reader is referred to the web version of this article.)

In the last decades, there has been much effort to understand carbon dioxide and water vapor fluxes and their controls based on eddy covariance towers (Baldocchi et al., 2001). However, the majority of these studies have investigated systems that were expected to be more productive and/or have greater potential for carbon sequestration, such as moist forests and crops (Running et al., 1999), while water-limited ecosystems, like dry forests, have been underrepresented (Buchmann and Schulze, 1999). Particularly in South America, CO_2 flux measurements are rather sparse and have been mostly devoted to the Amazonian forests. Recent studies have shown that dry forests, and particularly those from South America and Australia, can have a strong influence on the global carbon budget, even stronger than tropical rainforests (Poulter et al., 2014).

As in most water-limited ecosystems, rainfall, and consequently soil moisture, is a key driver of biological activity of South America dry forests (Contreras et al., 2011; Ferrero et al., 2013). However, the individual responses of different CO_2 fluxes (i.e. Gross Ecosystem Productivity, GEP; Ecosystem Respiration, R_{eco}) to rainfall and soil moisture are unknown in this kind of ecosystems, as well as their relative responsiveness to water inputs during dry and more dormant vs. wet and more active seasons. It is generally believed that in water-limited ecosystems, the net ecosystem exchange (i.e. NEE = R_{eco} – GEP) is positive during the dry season (i.e. carbon source), which means that respiratory CO_2 losses are higher than CO_2 accumulation fluxes; while the opposite occurs during the wet season (i.e. carbon sink) (e.g. Hastings et al., 2005; Luo et al., 2007; Scott et al., 2006). However, some evergreen shrubs (e.g. *Larrea divaricata)* and deep-rooted tree species which can be very abundant in the dry forests of southern South America (e.g. *Aspidosperma quebracho blanco*) may use water stored deeply in the soil (Gimenez et al., 2016; Jobbágy et al., 2008) being able to sustain low photosynthesis rates during rainfall shortage periods. Moreover, although it is acknowledged that higher rainfall inputs translate into higher primary productivity rates, the responses of respiration and photosynthesis fluxes to discrete and infrequent rainfall events (i.e. pulses, Schwinning and Sala, 2004) are not completely understood when shorter timescales (e.g. days, weeks) are considered, as they are highly dependent on the timing and magnitude of precipitation events (Huxman et al., 2004; Scott et al., 2009). Such knowledge is critical to improve global carbon budgets and ecosystem modeling, to predict climatic change impacts and to design management strategies.

Dry forests play also a key role in regional hydrological balances. Several studies worldwide have shown that evaporation from dry forests almost balances precipitation inputs, resulting in negligible deep drainage fluxes, deep water-table levels and large salt stocks in the vadose zone (Santoni et al., 2010; Scanlon et al., 2005; Seyfried et al., 2005). When crops or pastures replace dry forests, declines of evaporation rates and increases of deep drainage flux are commonly observed. In the long term, this has triggered the onset of groundwater recharge, water-table rise and soil salinization over large extensions (George et al., 1997; Leduc et al., 2001; Scanlon et al., 2005). Recent studies in Argentina confirm the exhaustive use of rainfall inputs in the long term leading to the presence of dry soil profiles with large salt stocks under dry forests (Amdan et al., 2013; Gimenez et al., 2016; Jayawickreme et al., 2011; Santoni et al., 2010). Yet, the short term behavior of water vapor fluxes in these ecosystems, their response to rainfall and soil moisture pulses and their link with the ecosystem CO_2 exchange are still poorly understood.

The main goals of this study were: a) to quantify for the first time the magnitude and temporal variability of CO_2 and water vapor exchange with the atmosphere from eddy covariance measurements in a dry forest of central Argentina, and b) to analyze how CO_2 and water vapor fluxes respond to different environmental factors, with focus on soil moisture and temperature. Given the arid conditions of the studied dry forest (mean rainfall is less than a quarter of mean potential evapotranspiration, $PP/ET_o = 0.23$), we hypothesize that soil moisture is the main driver of CO_2 and water vapor fluxes and that this influence exacerbates during the dry season. We also expected the forest to switch from a carbon source under the extreme aridity of the dry season ($PP/ET_o = 0.09$) into a carbon sink during the wet season ($PP/ET_o = 0.34$). We performed continuous measurements of CO_2 and water vapor during a 15-month period (Dec. 2009 – March 2011) in a representative dry forest stand in central Argentina. These measurements were complemented with field and satellite observations in order to evaluate the main environmental drivers of CO_2 and water vapor fluxes and to assess the leaf area seasonality of the site.

2. Materials and methods

2.1. Site description

The dry forest site (33.464 S; 66.459 W) is located in the centre of the San Luis province (Argentina) at an elevation of 500 m above sea level (Fig. 1), in the south extreme of the Chaco Dry Forest, close to the ecotone with the Monte (southern creosote bush) to the west and the Espinal (Southern mesquite woodland) to the south (Cabrera, 1976). The region presents a dry forest matrix with isolated patches of altered vegetation that include rainfed pastures of *Cenchrus ciliaris* and *Eragrostis curvula*, roller-chopped stands (only shrubs and small trees are removed), and to a much lesser extent irrigated plots of maize, sorghum and soybean (Marchesini et al., 2013; Steinaker et al., 2016). Extensive cattle raising represents the main economical activity in the region (Magliano et al., 2015c), with stocking rates of 0.05 and 0.2 calving units per hectare in native forest and pastures, respectively (Ser Beef S.A., personal communication). Firewood extraction is limited to homesteads and is rare around the study site.

2.2. Vegetation

The woody canopy of mature dry forest is principally dominated by two species, *Prosopis flexuosa* and *Aspidosperma quebracho-blanco*; the understory presents several shrub species such as *Larrea divaricata* and *Senna aphylla*, and perennial grasses such as *Stipa eriostachya* and *Aristida mendocina* (Table 1). We estimated a relative canopy cover of 82% and 51% for woody and grass species, respectively. The largest tree is *Aspidosperma quebracho-blanco* which can reach up to 12 m in height, followed by *Prosopis flexuosa* with 9 m. In the herbaceous layer, *Trichloris crinita* and *Setaria leucopila* are the preferred species for livestock, followed by the *Pappophorum caespitosum* and *Aristida mendocina*. *Prosopis flexuosa* and, to a lesser extent, *Larrea divaricata* are the woody species typically used as firewood. The large plant species diversity reported in Table 1, which is typical pattern of dryland ecosystems (Bisigato et al., 2009; Ludwig et al., 2005), is usually found in a small fraction of the landscape (< 1 ha) (Bogino and Bravo, 2014; Steinaker et al., 2016). It is also important to note that the species of Table 1 are also representative of the vegetation of other dry forests of central Argentina (Alvarez and Villagra, 2010; Britos and Barchuk, 2008).

2.3. Climate and soils

The climate is semiarid with a mean annual rainfall of 360 mm year^{-1} (1967–2009; Salinas del Bebedero, 15 km west from the study site and 2009–2017 own data on the study site) and Penman-Monteith-FAO potential evapotranspiration approaches 1500 mm year^{-1} (CRU, New et al., 2002). A typical year has 40 rainfall events, with the 8 largest ones (> 20 mm) accounting for 60% of total rainfall and the 22 smallest ones (< 5 mm) accounting for 7% of total rainfall (Magliano et al., 2015b). The mean annual temperature is 17.8 °C. The hottest (January) and coldest (July) months have average temperatures of 24.8 and 10.3 °C, respectively. The number of ground-frosts approaches 38 events per year, occurring typically between April and September (CRU, New et al., 2002).

Soils are well-drained and derived from fine loessic sediments deposited throughout the Holocene with some alluvial reworking (Iriondo, 1993; Tripaldi et al., 2013). Soils are Typic Torriorthents and Entic Haplustols with 53% sand, 15% clay, and 1.4% organic matter in the top 10 cm of the profile (Peña Zubiate et al., 1998; Toby Pennington et al., 2000). Topography is gentle with slopes < 1.5%. Water table is 30-m depth at the study site. Soil water monitoring (0–3 m depth) in dry forests of the study area show low and stable moisture levels in the dry winter and higher and more variable levels in the wet summer (Magliano et al., 2016; Marchesini et al., 2013). A list of soil and vegetation attributes derived from in-situ measurements in three forest stands at our study site are shown in Appendix Table A1.

Table 1
Relative frequency of species present in the studied dry forest grouped by layers according to their height: herbaceous (< 0.5 m), shrub (0.5–2 m) and tree (> 2 m). Species frequency was determined by interception transect lines (three 36-m lines for each layer). As this determination was based on the height of the plants, one species can appear in two different layers.

Herbaceus layer (<0.5 m)	%		Shrub layer (0.5-2 m)	%
Stipa eriostachya	34.5		***Larrea divaricata***	46.8
Aristida mendocina	32.0		*Senna aphylla*	14.3
Pappophorum ssp.	8.1		***Moya spinosa***	10.9
Cordobia argentea	6.9		*Celtis ehrembergiana*	10.8
Gouinia paraguayensis	3.9		***Condalia microphylla***	6.1
Abutilon terminale	2.8		***Capparis atamisquea***	4.8
Aristida adsencionis	2.6		*Prosopis flexuosa*	2.3
Celtis ehrembergiana	1.5		*Ximenia americana*	1.4
Trichloris crinita	1.4		*Lycium teneuspinossum*	1.3
Setaria leucophylla	1.3		***Schinus johnstonii***	0.9
Prosopis flexuosa	1.2		*Aloysia gratissima*	0.5
Lycium teneuspinossum	1.0			
Aloysia gratissima	0.8			
Condalia microphylla	0.6		Tree layer (>2 m)	%
Moss	0.5		*Prosopis flexuosa*	63.9
Moya spinosa	0.4		***Aspidosperma quebracho-blanco***	32.7
Schinus johnstonii	0.3		*Cercidium praecox*	3.4

Bold letter indicates evergreen shrubs and trees. Other species present in the study site, but not intercepted by transects, are the trees *Geoffroea decorticans* and *Bulnesia retama*.

2.4. Environmental measurements

Eddy covariance and environmental measurements were performed in the centre of a paddock of 1420 ha, which represents the typical dry forests of the region. Northwest to South winds (320° and 180°) prevail (87% of the time), offering a full dry forest cover fetch condition for about 1 kilometer. Upwind distance accounting for 80% of measured surface flux ranged between 76 and 334 m, as computed with Kljun's et al. footprint model (2004), indicating that the tower was well included in the fetch of the targeted cover. The study site belongs to a commercial ranch in which native forests are used for cattle grazing.

Above-canopy net radiation (NR) was measured using a net radiometer (NR-Lite, Kipp & Zonen, Delft, The Netherlands) mounted at ~4 m above the canopy. Also at this height, a photosynthetic photon flux density (SQ-110, Apogee Instruments, Logan, UT, USA) and solar radiation sensors (LI200S, LI-COR, Lincoln, NE, USA) measuring down welling radiation fluxes were installed. Ground heat flux (G) was measured using a soil heat flux plate (HFP01, Campbell Scientific, Logan, UT, USA) installed 5 cm below the surface in a representative location inside the patchy vegetation. The canopy heat storage (air and biomass) between the soil surface and the level of the eddy covariance instrumentation was not taken into account, since its importance is expected to be small in sites with short canopies and low biomass (Wilson and Baldocchi, 2000; Wilson et al., 2002) as the one we studied. The sum of all additional energy sources and sinks were also assumed to be negligible (Wilson et al., 2002).

Precipitation was quantified with a tipping-bucket gauge (TE525, Campbell Scientific, Logan, UT, USA) mounted at the top of the tower. We took advantage of an additional tipping-bucket gauge located ~1.9 km away from the tower to check the accuracy of precipitation measurements. Soil volumetric water content was measured by using FDR type sensors (ECH_2O-10 and EC-5 probes; Decagon Devices, Pullman, WA, USA) at 5, 10, 20 and 50 cm of depth beneath the tree canopy and in the proximity of the soil heat flux plate. These sensors did not work continuously and some gaps (~30% of the time series) were generated. Because the roots density declines with depth and roots extract water from soil in a non-uniform manner, we computed a representative metric of available soil moisture from 0 to 50 cm by weighting soil moisture by the probability distribution of roots by depth as proposed by Baldocchi et al. (2004). Root distribution by depth were taken from Marchesini (2011).

2.5. Eddy covariance measurements

A three-dimensional sonic anemometer (CSAT-3, Campbell Scientific, Logan, UT, USA) and an open-path infrared gas analyzer (LI-7500, LI-COR, Lincoln, NE, USA) were mounted 4 m above the dry forest canopy to measure the three components of wind velocity vectors (u, v and w), the sonic temperature, and the CO_2 and water vapor air concentrations. Measurements were undertaken for 15 months (12/21/2009 to 03/26/2011). Data were sampled at 20 Hz, controlled by Campbell Scientific CR1000 data logger (Campbell Scientific, Logan, UT, USA). The instrument was calibrated twice during the study period and its maintenance operations were performed following manufactureŕs recommendations. Half-hourly eddy fluxes were computed as the covariance between vertical wind velocity (w) and CO_2 (or water vapor) air concentrations using EVEDDY, a VBA (Visual Basic for Application) based software (Posse et al., 2014). Corrections for density fluctuations due to temperature and water vapor were applied by using the Webb-Pearman-Leuning procedure (Webb et al., 1980). The coordinate system was rotated using the planar fit method for sonic anemometer tilt correction (Wilczak et al., 2001).

Following FLUXNET standard procedures, data were post processed using EVEDDY (Posse et al., 2014), and including the following steps: despiking, night-time correction, flux partitioning and gap filling of half-hourly eddy fluxes. Firstly, half-hourly fluxes were filtered following two qualitative criteria: data were removed when precipitation events occurred, and/or when a stationary analysis indicated poor quality (Foken et al., 2004). Secondly, despiking was performed by removing half-hourly fluxes that were outside of a month to month variable range, and using quadratic regressions over a 10-day moving window. Thirdly, a three month period based critical friction velocity (u^*) threshold was used to exclude fluxes computed under calm wind conditions (Reichstein et al., 2005). After that, data rejection was 57.4%, 46.7% and 58.8% for carbon dioxide, latent heat and sensible heat fluxes, respectively. Fourth, a flux partitioning method was applied (Reichstein et al., 2005) to discriminate the ecosystem respiration (R_{eco}) from NEE, in order to quantify gross ecosystem productivity (GEP = R_{eco} − NEE). Finally, the gap filling procedure proposed by Reichstein et al. (2005) was implemented to allow computation of NEE, GEP and R_{eco} fluxes at time scales greater than a half-hour. The gap filling and random errors approached 1.6 and 1.8 g C m^{-2} for annual NEE, respectively and 2.9 and 2 MJ m^{-2} for the annual latent heat flux. The standard sign convention for NEE was used, whit NEE > 0 indicating net loss of CO_2 to the atmosphere (ecosystem acting as a source) and NEE < 0 indicating CO_2 uptake by the ecosystem (ecosystem acting as a sink), being R_{eco} and GEP always positive.

The system performance was assessed by statistically examining the energy balance closure (Wilson et al., 2002). The half-hourly values of latent heat flux (LE) plus sensible heat flux (H) were compared against available energy (net radiation (NR) minus soil heat flux (G)) by performing linear regression analysis. For the whole study period, the correlation was 86% (r^2 = 0.74) with an intercept value of 10.3 and a slope of 1.05 (slope of 1.07 with regression forced through origin), not statistically different from 1 ($p < 0.001$). The daily energy closure, evaluated as (H + LE)/(NR-G), approached 90%, similar to values reported for other sites (Wilson et al., 2002), evidencing a generally good performance.

2.6. Data analysis

In order to examine the association of CO_2 and water vapor fluxes with the environmental variables, the full dataset was divided into two seasons (i.e. dry and wet season) based on the monthly rainfall distribution. This distinction was done by taking into account the longest precipitation data set (1967–2009; Salinas del Bebedero meteorological station) located about 15 kilometers to the SW. There is a distinct dry season during the southern autumn and winter from May to September. During this 5-month period total precipitation represents on average an 8% of the annual total, with high interannual variability (temporal coefficient of variation of 122%). The rainy season extends from October to April; however, appreciable rain pulses are normally limited to November-March period, accounting on average for an 80% of the annual total. Intermittent dry spells are common during the wet season.

At the daily scale, we evaluated the association between CO_2 and water vapor fluxes with different environmental variables (soil moisture at different depths, soil temperature, air temperature, photosynthetically active radiation) using linear and non-linear regression models. We computed the Bowen Ratio (BR) and the Evaporative Fraction (EF), as the relationship between actual evapotranspiration and potential evapotranspiration ($ETactual/ET_o$), as indicators of vegetation water stress and analyzed their relationships with soil moisture. We evaluated the association between monthly CO_2 and water vapor fluxes with cumulative rainfall integrated over the current up to three previous months trough linear regression models.

We quantified the individual components of evapotranspiration (soil evaporation, transpiration and interception) using a simple hydrological model empirically derived from data collected in our study site (Magliano et al., 2017b). The model solves the ecosystem daily water balance considering the average canopy interception of dry forest of our study site (Magliano et al., 2016), and evaporation and transpiration dynamics (Magliano et al., 2017b). We run the model for the

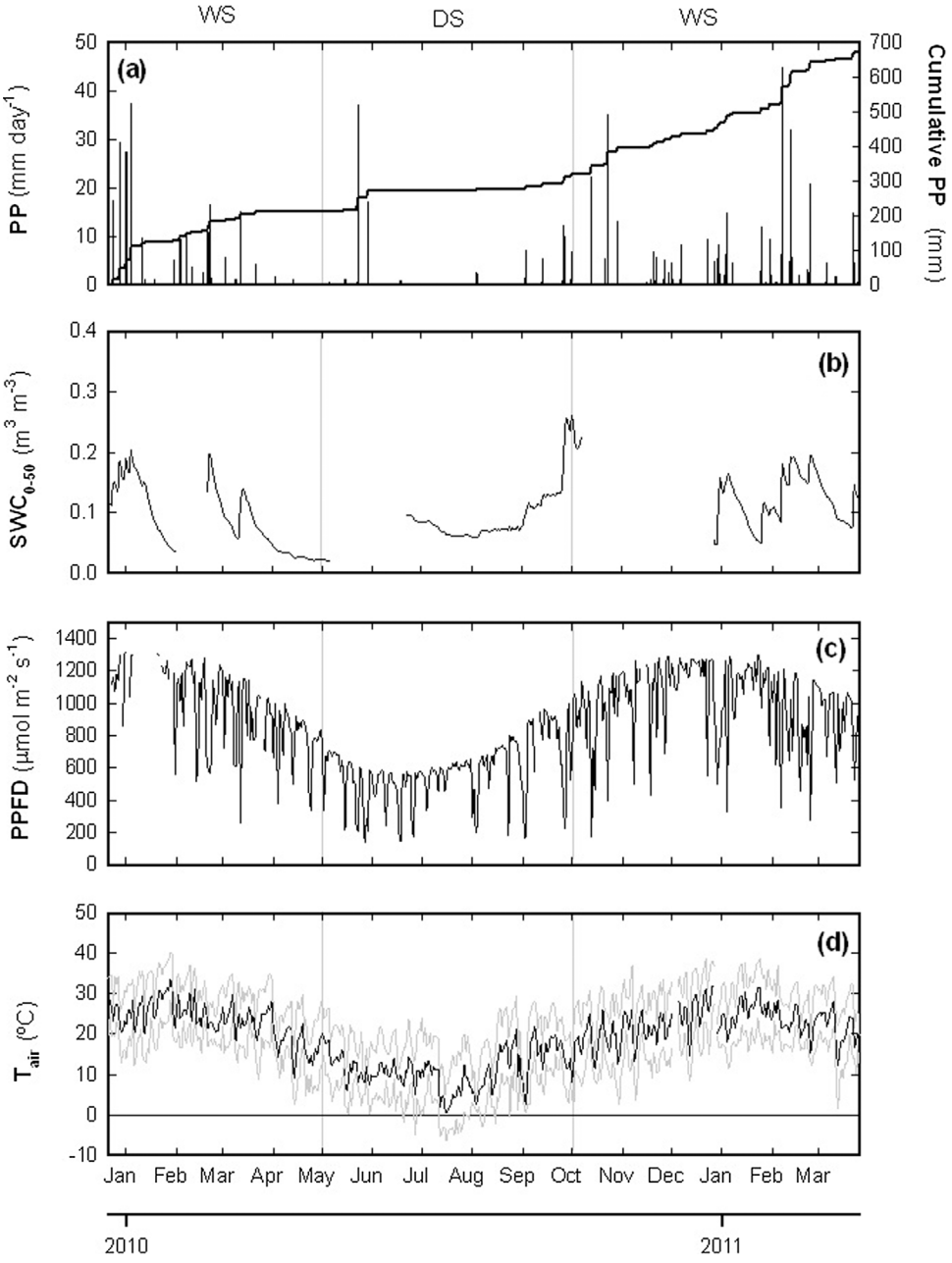

Fig. 2. Environmental conditions throughout the whole study period. (a) Daily total and cumulative precipitation (PP). (b) Daily soil water content for 0–50 cm depth ($SWC_{0–50}$). (c) Photosynthetic photon flux density (PPFD). (d) mean daily air temperature (T_{air}). In (d), air temperature with black line shows the daily mean and gray lines indicate daily minimum and maximum values. DS and WS at the top of the figure and vertical grey lines over each panel denote the extent of dry and wet seasons, respectively.

15-month period covered by the eddy covariance measurements.

3. Results and discussion

3.1. Meteorological conditions during study period

Precipitation during 2010 amounted to 421 mm, 15% more than the long-term annual average. Summer 2011 was the rainiest period, with February 2011 having a total monthly rainfall of 122 mm (twice the long-term monthly average; Fig. 2a). The 2010 dry season accounted for 24% of annual rainfall. An exceptional monthly rainfall of 57.4 mm was recorded in May 2010 (the 2nd for the period 1967–2010), which explained ~14% of annual rainfall.

Soil water content (SWC) between 0 and 50 cm of depth peaked following large precipitation events, with maximums reaching 0.20 $m^3\ m^{-3}$ and 0.26 $m^3\ m^{-3}$ during wet and dry seasons, respectively. During the wet season, SWC peaks were followed by steep decreases down to 0.03 $m^3\ m^{-3}$ at the end of April 2010 (Fig. 2b). By contrast, during the dry season one high rainfall event at the end of May of 37.2 mm, plus another moderate rainfall event six days later (17.2 mm), were enough to recharge the soil profile and keep SWC above 0.06 $m^3\ m^{-3}$ for the whole winter (Fig. 2b).

Photosynthetic photon flux density (PPFD) and air temperature (T_{air}) showed a strong seasonality (Fig. 2c and d). PPDF for clear days ranged between about 500 and 1300 μmol m^{-2} around winter and summer solstice, respectively. Frequency of overcast days was similar during the wet and dry seasons, with about 25% of days having clearness index K_T (ratio of measured vs. expected clear sky global solar radiation) lower than 0.8. Mean daily T_{air} ranged between 0 and 34 °C for the entire study period (Fig. 2d). The mean annual temperature for 2010 was 17.8 °C, very similar to the long-term average.

3.2. Annual and seasonal CO_2 and water vapor fluxes

The forest was a moderate carbon sink during the study period. Throughout 2010, the yearly integrated NEE approached

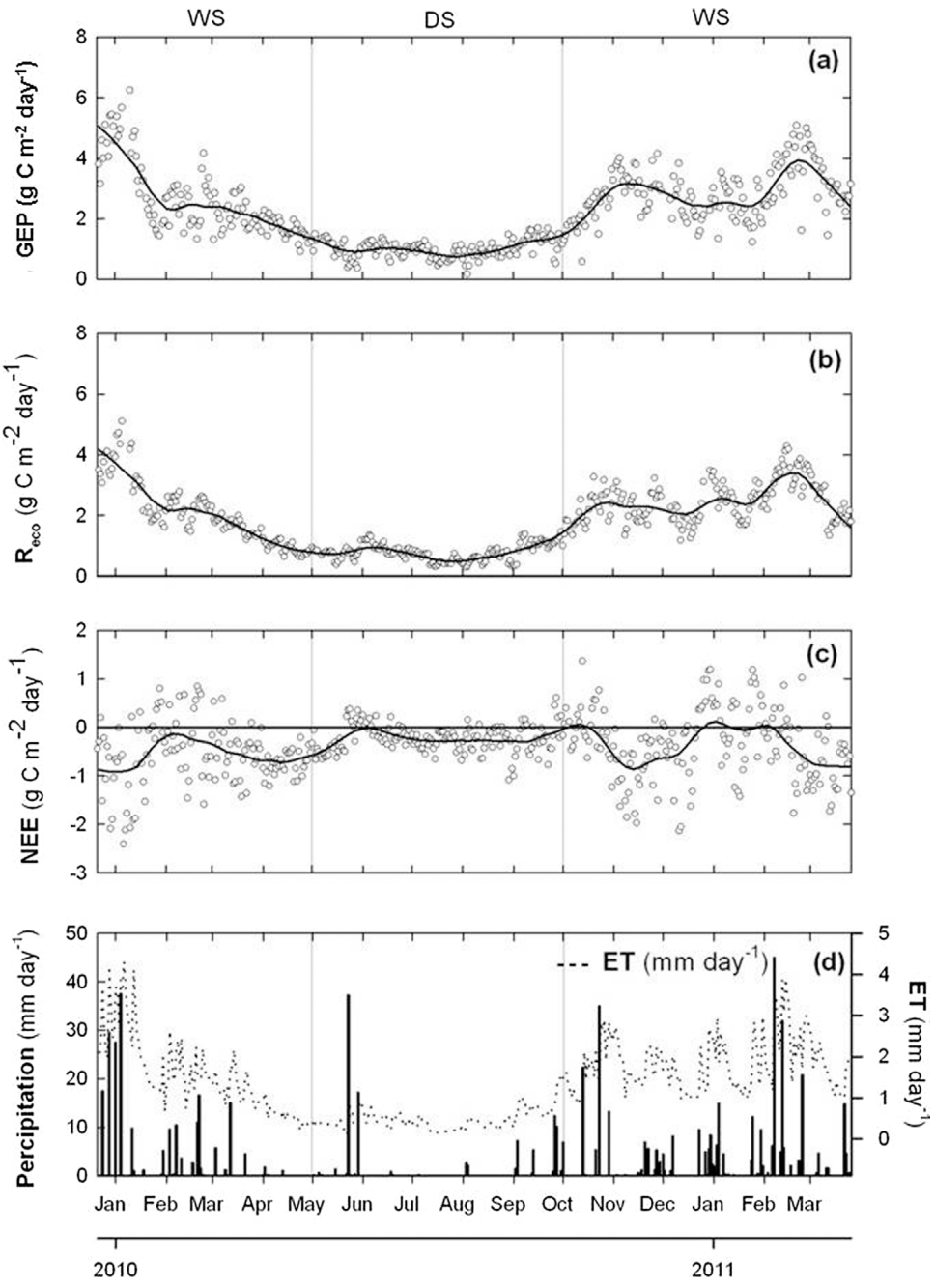

Fig. 3. Seasonal cycles of daily: (a) gross ecosystem productivity (GEP); (b) ecosystem respiration (R_{eco}); (c) net ecosystem exchange (NEE); and (d) precipitation and evapotranspiration (ET). Solid lines for each plot represent the data smoothed with a non parametric method for estimating regression surfaces (LOESS, performed in Sigma Plot 8.0, Systat Software, Inc.). DS and WS at the top of the figure and grey vertical lines over each panel denote the extent of dry and wet seasons, respectively.

-132.8 g C m^{-2} y^{-1} (-172.2 g C m^{-2} for the whole study period). The seasonal patterns of NEE revealed an unexpected, steady and significant sink of carbon during the cool dry season, accounting for a quarter of the total annual NEE of year 2010 (Fig. 3c). During this period, NEE ranged between -1.1 and 0.61 g C m^{-2} day^{-1} and averaged -0.23 g C m^{-2} day^{-1} (Fig. 3c) During the warm wet season, a highly variable but stronger (average = -0.44 g C m^{-2} day^{-1}) net CO_2 uptake was observed, yet frequent switches to net source were observed (Fig. 3c).

This first estimate of net CO_2 exchange for the second largest forest in South America after Amazonia should be considered with caution, given the less-than perfect energy balance closure, likely caused by measurement uncertainties, and also the limited time-span of the study. However, it is worth noting that the mean values of EVI (a surrogate of primary productivity derived from MODIS imagery, e.g. Sims et al., 2006) and soil moisture recorded during the study period (0.205 and 8.8%, for EVI and soil moisture, respectively) were similar to long-term means (0.21 and 8.5%, for EVI 13-years-average and soil moisture 5-years-average, respectively), which suggests that we captured a "normal" period in our study. In addition, results are comparable with aboveground primary productivity data estimated by biomass harvest at a similar site (NPP = 160 g C m^{-2} y^{-1}) (Braun et al., 1979). Besides, our NEE estimate is also comparable to other few estimates of annual carbon gains of semiarid woodlands in the world with similar annual rainfall: -96 to -155 g C m^{-2} y^{-1} for a semiarid chaparral in Southern California (Precipitation, PP = 349 mm y^{-1}, Luo et al., 2007); -212 g C m^{-2} y^{-1} (March to December only) for a semiarid riparian shrubland in Arizona (PP = 313 mm y^{-1}, Scott et al., 2006); -230 g C m^{-2} y^{-1} for a pine forest in southern Israel (PP = 285 mm y^{-1}, Rotenberg and Yakir, 2010); and -374 g C m^{-2} y^{-1} for a tropical dry forest in Northwest Mexico (May to November only, PP = 712 mm y^{-1},Perez-Ruiz et al., 2010).

The dry forests of the Southern Hemisphere, like the one we studied, are an important component of the global carbon balance. Recent

studies suggest that interannual variation on net CO_2 fluxes in semiarid areas of the Southern Hemisphere can have a superlative influence on the global carbon budget, explaining up to ~90% of global net primary productivity anomalies (Poulter et al., 2014). However, semi-arid ecosystems usually show high sensitivity to rainfall (Le Houerou et al., 1988) and drier periods may convert these areas in carbon sources (Verduzco et al., 2015), which is particularly important considering that many semi-arid ecosystems are experiencing decreasing rainfall trends (Biasutti, 2013; Cai and Cowan, 2012). These processes seem to be poorly represented in Earth System Models so far (Poulter et al., 2014).

Partitioning NEE into its component fluxes showed that the dry forest had a year-round growing season. It showed low but constant gross ecosystem productivity (GEP) rates during winter (July – September) that averaged 1 g C m^{-2} day^{-1} and peaked during spring, summer and early autumn (Fig. 3a). During the dry season, the GEP accounted for a quarter of the annual gross CO_2 uptake of the ecosystem. Ecosystem respiration (R_{eco}) followed GEP patterns throughout the year with minimums during winter season (on average 0.73C m^{-2} day^{-1}) and maximums during summer months (Fig. 3a and b). R_{eco} during the dry season represented 23% of the annual flux.

Evergreen species are likely making a larger contribution to the annual gross ecosystem productivity than deciduous ones. We estimated the contribution of deciduous and evergreen species to the gross CO_2 uptake through two different approaches. On the one hand, we took into account the leaf area seasonality (LAI, derived from MODIS imagery, product MOD15A2) and assumed that the leaf area observed during the dry season (which is only associated to evergreen species) remains constant during the wet season and that the increase in LAI during this season corresponds to the contribution of the deciduous species. On the other hand, we used data of canopy cover of these two vegetation groups estimated during the wet season. Both approaches yielded similar results and suggested that evergreen species accounted for between 56% (LAI method) and 67% (canopy cover method) of gross annual CO_2 uptake.

Cumulative ecosystem water vapor flux during the study period accounted for most of accumulated rainfall. Precipitation (PP) over the study period was 674 mm, and more than 88% of it returned to the atmosphere through evapotranspiration (ET = 595 mm) (Fig. 3d). Given that no differences were observed in stored soil water for the first 0.5 m of the profile between the beginning and end of the study period, it is possible that the difference between both water fluxes (PP – ET = 79 mm) indicates an increase of soil water below that depth and/or runoff. The first possibility is very likely considering that the beginning of the study period was preceded by a dry period (PP 35% below the average in the previous 9 months) and that in two rainfall event the wetting front reached 0.5 m depth of the soil profile (Fig. 2b). Runoff water losses are likely minimal in the study site, even during high precipitation events, as shown by existing field studies close to the study site (Magliano et al., 2017a; Magliano et al., 2016).

A simple hydrological model suggested that transpiration was the main process contributing to evapotranspiration. Vegetation transpiration accounted for 66.9% of total evapotranspiration, followed by canopy interception (19.7% of total ET) and soil evaporation (13.4% of total ET). These results are consistent with other studies in dry forests (Köstner, 2001; Raz-Yaseef et al., 2010) and shrublands (Scott et al., 2006; Stannard and Weltz, 2006) showing that transpiration is the largest component of ET. The dominant role that transpiration plays in the water losses of these ecosystems is already evidenced by the strong hydrological consequences generated by deforestation and transpiration reductions in the region (Contreras et al., 2013; Gimenez et al., 2016).

Daily CO_2 fluxes during the 2009–2010 wet season mirrored rainfall trends. At the start of the measurement period, by the end of December 2009, the dry forest consistently showed NEE rates of up to -2.4 g C m^{-2} day^{-1}. The highest rates of GEP and R_{eco} (6.2 g C m^{-2} day^{-1} and 5.1 g C m^{-2} day^{-1}, respectively) were observed during this period (Fig. 3a and b), probably associated to four precipitation events that accounted for a total of 112 mm (75.3% higher than the long-term average for December) just in a 12-day time interval (Fig. 2a). After these heavy rains, GEP and R_{eco} decreased steeply following the reduction in soil water content (Fig. 2b). The more pronounced reduction in GEP than in R_{eco} determined an increasing NEE that turned the dry forest from a near neutral to a slight source of carbon (up to 0.85 g C m^{-2} day^{-1}) many days during midsummer. Just after rainfall became more regular by early February 2010, and the soil was wetted again, GEP and R_{eco} stopped declining so steeply. During March and April, a steeper reduction of R_{eco} than GEP resulted in a consistent sink of carbon during late wet season, even when leaf fall of some tree species had started and available soil water had been depleted (Fig. 2b).

Daily CO_2 fluxes during the dry season showed much lower variability than during the wet season. At the onset of the dry season, and triggered by a large rainfall event at the end of May (Fig. 3d), there was a short period when the ecosystem was a small source of carbon to the atmosphere (with maximum fluxes of 0.37 g C m^{-2} day^{-1}; Fig. 3c). Just after that and even when leaf area and photosynthesis activity have already reached their minimums (0.7 g C m^{-2} day^{-1}, respectively), the ecosystem was a small but significant and constant sink of carbon, with maximum uptake rates of around -1.1 g C m^{-2} day^{-1} (Fig. 3a and c). This net uptake of CO_2 remained so until the leaf development onset and the arrival of first heavy rains by October, when R_{eco} peaked and dominated the carbon balance for a few days (Fig. 3c and d).

A more detailed scrutiny of daily pattern shed light on the effects of rain pulses on CO_2 fluxes. During summer, dry spells of several days accompanied by high vapor pressure deficits caused declines in GEP and positive NEE (e.g. at the end of January 2010, Fig. 3). Rain events during the summer intensified CO_2 release by a few days, due to an immediate increase in respiration plus a drop in GEP because of the low radiation, but then reversed them, switching the dry forest to sink, due to a later increase in GEP (e.g. from mid to end of February, Fig. 3). During winter, long dry spells did not cause declines in GEP nor turn the dry forest into a net carbon source as seen during summer, and most of positive values in NEE during this period corresponded to cloudy days (Fig. 3).

On average, daily water vapor fluxes (i.e. evapotranspiration, ET) during the wet season were almost fourfold those observed during the dry season (1.7 mm d^{-1} vs. 0.45 mm d^{-1}, respectively, Fig. 3d). Mean daily ET always peaked in response to rainfall events, being the responsiveness higher during the warm wet season and hence the variability (Standard Deviation = 0.8 mm d^{-1} and 0.25 mm d^{-1} for wet and dry season, respectively). During summer, maximum ET values followed rainfall event, after which ET rates abruptly drop till the next rainfall event. This drop was faster when the size of the rainfall event was smaller. For example, a 15 mm event in March 2010 increased ET for five days until reaching the pre-rain ET values, while 10 mm events in January and February 2010 increased ET for only two days. During the dry winter, ET peaks were also observed after rainfall event, but in this case the falling rates after the event were lower than in the wet season (Fig. 3d). At the end of the 2010 wet season and beginning of the dry season, when the first 0.5 m of the soil profile were completely dry (Fig. 2b), ET rates remained around 0.35 mm d^{-1} (Fig. 3d) indicating the use of deep water sources by the vegetation.

Rainfall events generated strong responses in ecosystem fluxes evidencing a pulsed behavior of them (Fig. 3). In agreement with the conceptual pulses model (Huxman et al., 2004), after a rainfall event, a rapid increase in CO_2 release was observed, which would respond to increase in microbial activity and physical displacement of CO_2 accumulated previously in the soil matrix. This CO_2 flux outweighs the increase in CO_2 fixation by photosynthesis for a few days, but then there is a net carbon gain. Beside this pattern already documented in other semiarid ecosystems (Jenerette et al., 2008; Kurc and Small, 2007), it is

interesting to note that during the longest dry spell (only 5 mm of rainfall in three months, June-August), the dry forest was able to sustain a constant and steady CO_2 uptake flux ($\sim 1\ g\ C^{-2}\ m^{-2}\ d^{-1}$) and behave as a carbon sink, evidencing high adaptation to arid conditions.

The observed CO_2 uptake pattern suggests two combined dynamics, whit rapid responses to rainfall events overlaid over a more stable, baseline behavior. This likely results from the coexistence of deciduous tree species and shallow rooted grasses (e.g. *Prosopis flexuosa, Setaria leucopila*, *Stipa eriostachya*), with fast responses to rainfall events, and deep rooted evergreen woody species (e.g. *Aspidosperma quebracho-blanco*, *Larrea divaricata, Condalia microphilla*), with slower but more stable responses during inter-pulses periods (Golluscio et al., 2009; Ogle and Reynolds, 2004; Sala and Lauenroth, 1982). The biological activity of these drought-adapted species determines that during the dry season the dry forest behaves as a net and steady carbon sink, as opposed to what has been observed in other semi-arid ecosystems (Brümmer et al., 2008; Hastings et al., 2005). It is also likely that these species, by sustaining transpiration during the dry season, have a key role in generating the zero drainage condition typical of these ecosystems (Santoni et al., 2010), as they would promote the drying of the soil profile to deep layers. The disruption of this zero drainage condition, which occurs both with deforestation for agriculture and with the removal of shrubs with roller-chopping (Marchesini et al., 2013; Santoni et al., 2010), is the main cause of serious dryland salinization problems in this and other dry forest ecosystems of the world (George et al., 1997; Marchesini et al., 2016).

3.3. Daily cycles of CO_2 fluxes

Clear diurnal patterns of CO_2 fluxes were observed during both the dry and wet seasons, but stronger amplitudes were observed during the summer wet season (Fig. 4). In the cool dry season, the dry forest started to assimilate CO_2 one hour after sunrise, at 8:00, and became a carbon sink from 9:00 h to 18:00 h. Maximum GEP rates (0.14 mg $CO_2\ m^{-2}\ s^{-1}$) occurred around 13:00 h, at the same time that maximum PAR flux. During the wet season, CO_2 assimilation peaked one hour before the maximum PAR flux (0.29 mg $CO_2\ m^{-2}\ s^{-1}$ at 11:30 h) and the dry forest was a net sink of carbon from 8:00 h to 19:00 h, with a maximum NEE rate of -0.19 mg $CO_2\ m^{-2}\ s^{-1}$ at 11:30 h. Maximum rates of R_{eco} coincided with maximum air temperature in both seasons (Fig. 4b).

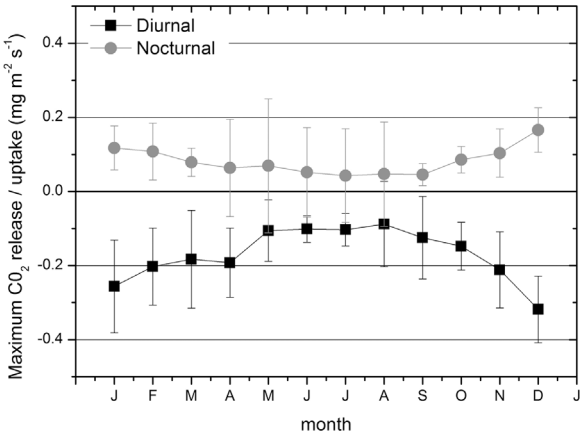

Fig. 5. Seasonal variation of maximum CO_2 release during the night and net uptake during the day. Vertical lines indicate the standard deviation.

Seasonal variations of daily maximum net CO_2 uptake during the day and CO_2 release during nighttime provide insights about the seasonality of the carbon sequestration potential of this dry forest. The maximum uptake rate during the day remained rather stable during dry season months (-0.1 mg C $m^{-2}\ s^{-1}$, Fig. 5). With the onset of the wet season, the maximum uptake rate increased and peaked in December (-0.32 mg C $m^{-2}\ s^{-1}$, Fig. 5). This value is lower than those observed for deciduous forests and is located at the lower limit within evergreen forests, being only similar to Mediterranean oaks forests (*Adenostoma ceanothus*) and black spruce forests (Brümmer et al., 2008; Falge et al., 2002; Wofsy et al., 1993). The maximum CO_2 nighttime release was in phase with the maximum CO_2 uptake, showing December the highest value (0.16 mg C $m^{-2}\ s^{-1}$, Fig. 5). The maximum CO_2 nighttime release was also similar to values observed for evergreen oak forests and much lower than those of other evergreen and deciduous forests (Falge et al., 2002). However, the lowest monthly value of the maximum CO_2 uptake during the day (- 0.09 mg C $m^{-2}s^{-1}$ in July, Fig. 5) was notably higher than rates reported for deciduous forests and similar to those

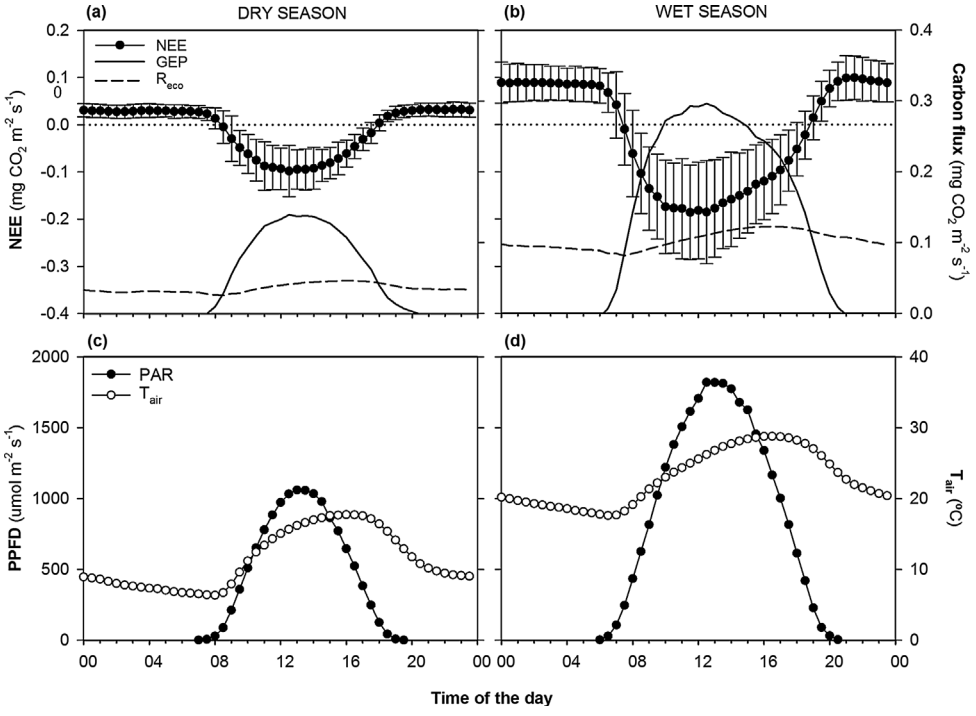

Fig. 4. Daily cycles of (a–b) net ecosystem exchange (NEE), gross ecosystem productivity (GEP), and ecosystem respiration (R_{eco}); (c – d) photosynthetic active radiation (PAR) and air temperature (T_{air}) for dry and wet seasons.

Table 2
Coefficients of determination (r^2) of linear regression models adjusted between daily CO_2 (R_{eco} and GEP) and water vapor fluxes and environmental variables. Only clear sky days were considered in this analysis.

		Wet Season			Dry Season		
	Depth	ET	R_{eco}	GEP	ET	Reco	GEP
Soil Moisture	5 cm	0.69	0.58	0.45	**0.56**	0.48	0.28
	10 cm	0.70	0.63	0.54	0.41	0.41	0.27
	20 cm	0.50	0.50	0.57	0.33	0.35	0.29
	50 cm	0.29	0.37	0.40	0.34	0.21	0.18
	0–50 cm	**0.78**	**0.77**	**0.73**	0.44	0.40	0.28
Soil Temperature	5 cm	*0.00*	0.10	*0.03*	0.30	0.40	0.48
	10 cm	*0.00*	0.06	*0.00*	0.50	**0.63**	**0.59**
	20 cm	*0.00*	0.06	*0.00*	0.31	0.35	0.46
	50 cm	0.08	0.11	*0.04*	*0.00*	*0.00*	0.08
	0–50 cm	*0.00*	0.07	*0.00*	0.30	0.36	0.46
Air Temperature		*0.01*	0.19	*0.01*	0.14	0.54	0.39

Numbers in italics indicate when models are not statistically significant ($p < 0.01$) and in bolds indicate the highest coefficients.

observed in temperate evergreen forests (Falge et al., 2002).

3.4. Biophysical controls of CO_2 and water vapor fluxes

As expected for a semi-arid ecosystem, soil moisture had a strong influence on the carbon balance, with clearer effects during the warm wet season (Table 2). During the wet season, daily CO_2 fluxes (R_{eco} and GEP) were strongly associated with the soil moisture; the best fit was achieved considering soil moisture of the whole soil profile (0–50 cm). On the other hand, during the dry season the influence of soil moisture on the CO_2 fluxes was notoriously lower, while soil temperature became an important driver, explaining up to 63% and 59% of Reco and GEP variability, respectively. By contrast, the influence of temperature on CO_2 fluxes was not significant during the wet season. The leaf area index (derived from MODIS imagery) and the photosynthetically active radiation had a markedly lower influence on daily GEP fluxes than the most important drivers of soil moisture and temperature for the wet and dry season, respectively. In contrast to the definition of dry and wet season, this analysis suggests that during the dry season, which includes the southern autumn and winter (T_{air} mean = 11 °C), temperature is the main control of biological activity, whereas during the wet season (T_{air} mean = 22 °C) it is soil moisture.

Daily evapotranspiration was strongly associated with soil moisture during both wet and dry seasons (Table 2). In the wet season, evapotranspiration was best explained (r^2 = 0.78) by the water content of the whole soil profile (0–50 cm), while in the dry season the best adjustment (r^2 = 0.56) was achieved considering top soil moisture (0–5 cm). We also found that in the dry season soil temperature strongly affected evapotranspiration (r^2 = 0.50 considering measurements at 10 cm-depth), but its influence was marginally significant during the wet season.

The evaporative fraction (EF = ET_{actual}/ET_o) and the Bowen Ratio (BR) were strongly associated with soil moisture, suggesting pervasive water stress conditions in the studied ecosystem (Fig. 6). We found that the EF was higher and strongly associated to soil moisture in the wet season (0.28 vs. 0.19 for WS and DS, respectively) (Fig. 6a). Interestingly, the relationship between EF and soil moisture during the wet season was best explained by a bi-linear model with a breakpoint at 9% of soil moisture. The BR can be used as an indicator of water stress because as vegetation experiences drought, a higher proportion of available energy dissipates as sensible heat rather than latent heat, increasing BR. As in the case with the EF, we found a stronger and linear association with soil moisture during the wet season (Fig. 6b). Given that we did not find a saturation response of the EF or BR vs. soil moisture as it would be expected if soil moisture were not the limiting

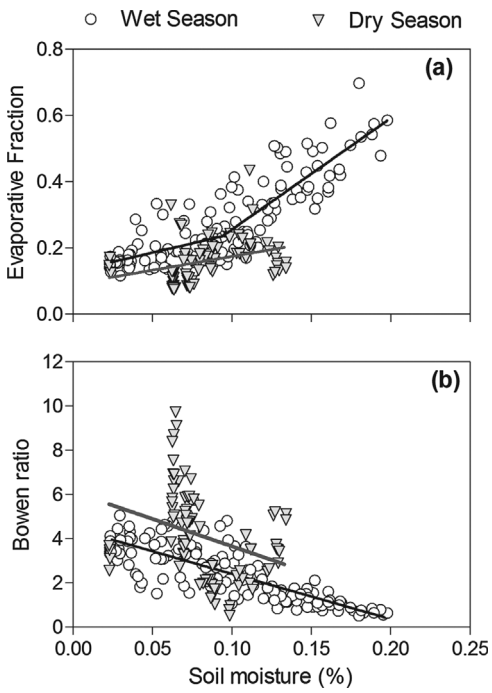

Fig. 6. Relationships between daily Evaporative Fraction (ET_{actual}/ET_o, Panel a) and Bowen Ratio (Panel b) with soil moisture for dry and wet seasons. Only clear sky days were considered in this analysis.

factor of ET (Bracho et al., 2008), we speculate that vegetation is in a permanent water stress condition. We did not find any significant relationship between LAI (derived from MODIS imagery) and the BR, as it has been observed in other ecosystems (Bracho et al., 2008; Jia et al., 2016).

At the monthly scale, rainfall had a strong influence on CO_2 and water vapor fluxes only during the wet season (Table 3). During this period, current-month rainfall accounted for 35% of the variability of GEP ($PP_{month\ i}$ vs $GEP_{month\ i}$), but this amount increased notably to 65% when the rainfall of the previous month was included in the calculations ($PP_{months\ i+i-1}$ vs $GEP_{month\ i}$). In the case of R_{eco} and ET, the addition of the rain of the previous month did not produce an improvement in the amount of variability explained by the models. This pattern suggests a lag in the response of vegetation to rainfall inputs, as it has already been observed in other arid ecosystems (Sala et al., 2012; Yahdjian and Sala, 2006).

The efficiency of net and gross CO_2 exchange relative to that of water evaporated increased as the soil dried in both seasons, yet the relationships were different between them (Fig. 7). This increase in the ecosystem water use efficiency as soil moisture declines suggests a lower relative importance of soil evaporation on total evapotranspiration as time progresses after rainfall events. Interestingly, the time span during which the carbon efficiency increases after a rainfall event is

Table 3
Coefficients of determination (r^2) of linear regression models adjusted between monthly fluxes of CO_2 (R_{eco} and GEP) and water vapor and rainfall integrated for different time periods (from 1 up to 3 months).

	Wet Season			Dry Season		
Rainfall	ET_i	$R_{eco,\ i}$	GEP_i	ET_i	$R_{eco,\ i}$	GEP_i
month i	0.69	0.68	*0.35*	*0.19*	*0.16*	*0.28*
month i + i-1	0.68	0.68	0.65	*0.27*	*0.50*	*0.28*
month i+ i-1 + i-2	*0.36*	*0.30*	*0.34*	*0.00*	*0.25*	*0.00*

Numbers in italics indicate when models are not statistically significant ($p < 0.05$, $n = 10$ for WS and $n = 5$ for DS).

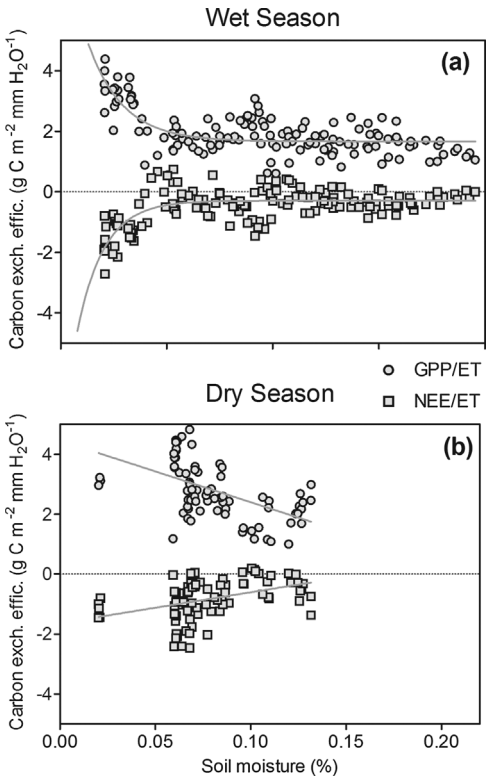

Fig. 7. Relationships between carbon exchange efficiencies (GPP/ET and NEE/ET) with soil moisture for wet (a) and dry (b) seasons. Only clear sky days were considered in this

remarkably long, exceeding a month (data not shown), which is in agreement with recent observations in the study site that show low soil evaporation rates that extend the period during which soil evaporation occurs (Magliano et al., 2017b). On the other hand, as the period without rains spreads and drought conditions intensify, leaf-level adjustments may occur (i.e. changes in leaf conductance and carboxilation capacity) that may also increase the ecosystem water use efficiency (Grünzweig et al., 2003; Reichstein et al., 2002).

Half-hourly CO_2 fluxes were strongly affected by air temperature, although its effect differed between the dry and wet seasons (Fig. 8). During the dry season, temperature increases between 5 °C and 31 °C resulted in consistent increases in GEP and R_{eco}, which finally determined no significant variation in NEE. During the wet season, temperature increases between 12 °C and 25 °C also produced similar increases in GEP and R_{eco}, and no significant trend in NEE. However, above 26 °C GEP experienced a sharp decline from ~7.7 mg CO_2 m^{-2} s^{-1} (at 25 °C) to 2.4 mg CO_2 m^{-2} s^{-1} (at 40 °C), while R_{eco} showed first a slight increase, up to 32 °C (3.3 mg CO_2 m^{-2} s^{-1}), and then a slow reduction that stabilized at around 2.7 mg CO_2 m^{-2} s^{-1} (at 39 °C). Evapotranspiration also abruptly fell above 26 °C during the wet season which suggests the onset of stomatal closure. The different responses for GEP and R_{eco} determined an abrupt decline in net ecosystem exchange rates, from −0.2 mg CO_2 m^{-2} s^{-1} to 0.01 mg CO_2 m^{-2} s^{-1} for temperatures between 27 °C and 40 °C.

The observed responses of CO_2 fluxes to air temperature partially agree with previous observations in other ecosystems. The switch from carbon sink to carbon source that occurred between 26 °C and 40 °C was not due to increased maintenance respiration as it has been observed by other authors (Adams et al., 2009; Atkin and Tjoelker, 2003;

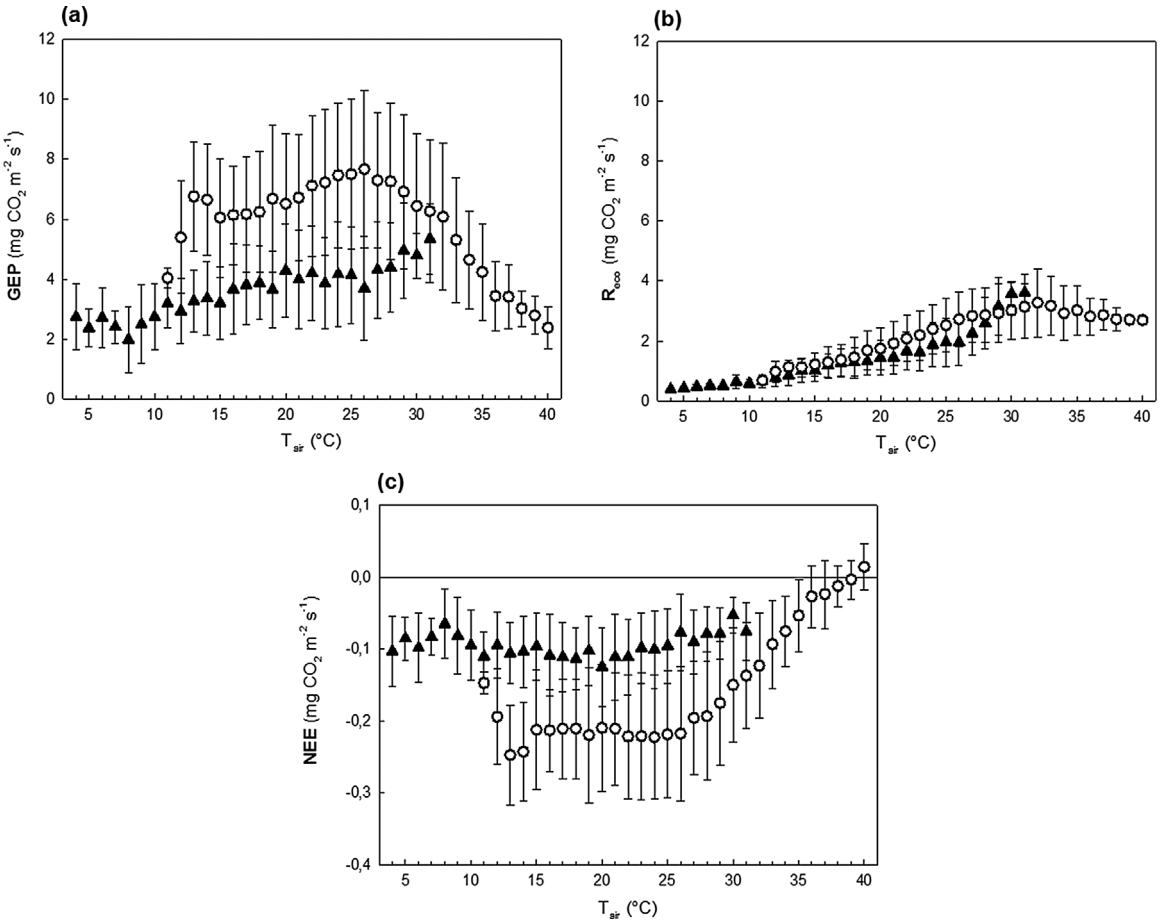

Fig. 8. Relationships between (a) gross ecosystem production (GEP), (b) ecosystem respiration (Reco) and (c) net ecosystem exchange (NEE) with air temperature. Relationships are shown for wet (circles) and dry (triangles) seasons separately. Vertical lines indicate the standard deviation.

Zhao et al., 2013), since R_{eco} changes were small in this temperature range (Fig. 8b), but to an abrupt fall in CO_2 uptake rates (Fig. 8a) (Bernacchi et al., 2001). This pattern was not observed in the dry season with temperatures above 26 °C. Higher soil moisture contents could reduce the effect of thermal stress (Zhao et al., 2013) but this would not be the case in our system since soil moisture was, on average, similar in both seasons. Maybe, a higher relative preponderance during the dry season compared to the wet season of the most prevalent warm desert evergreen shrub *Larrea divaricata*, which is well adapted to high temperatures (Salvucci and Crafts-Brandner, 2004), is explaining the observed pattern. Considering our observations and the climate change context, it results highly important to quantify carefully the effects of temperature rise on the carbon balance of this and other dry forest ecosystems.

4. Summary and conclusions

Based on eddy covariance technique, we provide key findings that expand our knowledge about carbon and water dynamics and their environmental controls in the studied ecosystem. We found that the dry forest was a net carbon sink during the study period (15 months) even during the very dry season, which differs from our hypothesis and from many other studies that show ecosystems behaving as carbon sources during drought periods. As we previously hypothesized, soil moisture was a main control of daily fluxes of CO_2 and water vapor but its influence was markedly higher during the warm wet season. Unexpectedly, soil moisture (and rainfall) had a lower influence on CO_2 fluxes during the cool dry season, with temperature becoming the dominant driver in this period. Overall, the CO_2 uptake dynamics showed two overlapping patterns directly related with rainfall inputs. On the one hand, we observed a CO_2-pulses pattern triggered by rainfall events, where CO_2 uptake peaks immediately after rain and then declines sharply. This supports the "trigger-transfer-pulse-reserve" framework, developed for water-limited ecosystems, which postulates that the whole ecosystem depends principally on (and is triggered by) rainfall inputs. On the other hand, we found a basal and steady CO_2 uptake pattern that operates during rainless period, likely sustained by evergreen drought tolerant species (e.g. *Larrea divaricata*). Interestingly, agricultural management (e.g. grazing, prescribed fire, roller-chopping) may change the relative proportion of plant functional groups (e.g. Steinaker et al., 2016), and by doing this, the relative importance of pulsed vs. basal CO_2 patterns.

Acknowledgements

This work was funded by grants from ANPCyT (PICT 2790/14, PICT 1840/06, Argentina), UBACyT (N° 20020100100736), CONICET (PIP 112-201501-00609) and the International Development Research Center (IDRC 106601-001, Canada). We also want to thank to Vicky Marchesini for providing us with soil moisture data and two anonymous reviewers and the associated editor for their helpful comments to improve the manuscript. Garcia A, Houspanossian J and Magliano P were supported by CONICET Fellowships.

Appendix A

Soil and vegetation attributes

Leaf area index above 25 cm and 150 cm height and incident radiation (n = 54) at the corresponding positions were estimated using hemispherical photographs obtained with a Nikon Coolpix 5400 camera fit with a FC-E9 Fisheye lens (Nikon, Tokyo, Japan) (Breshears and Ludwig, 2010). Digital photos were analyzed using Delta-T HemiView software (HemiView 2.1, Delta-T Devices, Cambridge, UK) (Rich et al., 1999). Soil litter cover was determined by visual interpretation of photographs of an area of 1 m^2 of the ground surface. Soil litter depth was determined by measuring and averaging the thickness of the litter layer from the mineral soil surface to the top, at eight random points. Microtopography was determined by measuring height differences between a central point (n = 54) and four neighbors points (located 0.5 m away in the N, S, E, and W directions), using a Ziplevel Pro-2000 altimeter, with a 2-mm resolution (Technidea, Escondido, CA). Penetration resistance was measured using an analog pocket penetrometer (Eijkelkamp, Gelderland, Netherlands) and infiltration rate was determined with the double-ring method (Eijkelkamp, Giesbeek, Netherlands). We report the infiltration rate in saturation conditions, a measure independent of prior soil water content (Wilson and Luxmore, 1988). Bulk density and water holding capacity (0–10 cm) were determined using the same field samples. For this purpose, we irrigated each patch with ~50 mm of water and we immediately covered it with polyethylene film in order to avoid evaporation. Twenty-four hours later, we took soil samples from the upper 10 cm using the cylinder method (Grossman and Reinsch, 2002; Hillel, 1998) and determined bulk density values in the laboratory by dividing the dry soil weight (dried for 72 h at 105 °C) by the volume of the cylinder. We estimated the initial water content of each soil sample as the water content at field capacity. More methodological details can be found in Magliano et al. (2015a; Magliano et al. (2015a; 2017a).

Table A1
Summary of soil and vegetation attributes of dry forests of the study area.

Biophysical attributes	units	mean	median	min	max	CV
LAI above 25 cm height	index	1.0	0.9	0.3	2.2	41.5
LAI above 150 cm height	index	0.6	0.5	0.1	1.5	56.5
Incident radiation above 25 cm height	%	47.5	46.9	0.2	0.9	38.7
Incident radiation above 150 cm height	%	31.0	33.0	0.3	1.0	65.6
Soil litter cover	%	44.9	37.5	0.0	100.0	64.6
Soil litter depth	cm	0.8	0.5	0.0	3.3	92.0
Microtopography	cm	5.0	4.8	0.5	11.0	13.4
Penetration resistance	kg/m^2	1.9	1.5	0.6	5.0	49.3
Infiltration rate	mm/h	172.0	128.0	24.0	834.0	80.6
Bulk density	g/cm^3	1.2	1.3	0.7	1.4	3.4
Water holding capacity 0–10 cm depth	%	17.1	18.7	10.7	26.0	6.5
Water holding capacity 10–20 cm depth	%	20.6	20.9	16.3	23.9	10.4

References

Adams, H.D., et al., 2009. Temperature sensitivity of drought-induced tree mortality portends increased regional die-off under global-change-type drought. Proc. Natl. Acad. Sci. 106 (17), 7063–7066.

Alvarez, J.A., Villagra, P.E., 2010. Prosopis flexuosa DC. (Fabaceae, mimosoideae). Kurtziana 35, 47–61.

Amdan, M.L., Aragón, R., Jobbágy, E.G., Volante, J.N., Paruelo, J.M., 2013. Onset of deep drainage and salt mobilization following forest clearing and cultivation in the Chaco plains (Argentina). Water Resour. Res. 49 (10), 6601–6612.

Atkin, O.K., Tjoelker, M.G., 2003. Thermal acclimation and the dynamic response of plant respiration to temperature. Trends Plant Sci. 8 (7), 343–351.

Baldocchi, D., et al., 2001. FLUXNET: a new tool to study the temporal and spatial variability of ecosystem-Scale carbon dioxide, water vapor, and energy flux densities. Bull. Am. Meteorol. Soc. 82 (11), 2415–2434.

Baldocchi, D.D., Xu, L., Kiang, N., 2004. How plant functional-type, weather, seasonal drought, and soil physical properties alter water and energy fluxes of an oak-grass savanna and an annual grassland. Agric. For. Meteorol. 123 (1-2), 13–39.

Bernacchi, C.J., Singsaas, E.L., Pimentel, C., Portis Jr, A.R., Long, S.P., 2001. Improved temperature response functions for models of Rubisco-limited photosynthesis. Plant Cell Environ. 24 (2), 253–259.

Biasutti, M., 2013. Forced Sahel rainfall trends in the CMIP5 archive. J. Geophys. Res.: Atmos. 118 (4), 1613–1623.

Bisigato, A.J., Villagra, P.E., Ares, J.O., Rossi, B.E., 2009. Vegetation heterogeneity in Monte Desert ecosystems: a multi-scale approach linking patterns and processes. J. Arid Environ. 73 (2), 182–191.

Bogino, S., Bravo, M., 2014. Impacto del rolado sobre la biodiversidad de especies leñosas y la biomasa individual de jarilla (Larrea divaricata) en el Chaco Árido Argentino. Quebracho 22, 79–87.

Bracho, R., et al., 2008. Environmental and biological controls on water and energy exchange in Florida scrub oak and pine flatwoods ecosystems. J. Geophys. Res.: Biogeosci. 113 (G2). http://dx.doi.org/10.1029/2007JG000469.

Braun, R., et al., 1979. Productividad primaria aérea neta del algarrobal de Ñacunan (Mendoza). Deserta 5, 7–73.

Breshears, D.D., Ludwig, J.A., 2010. Near-ground solar radiation along the grassland-forest continuum: tall-tree canopy architecture imposes only muted trends and heterogeneity. Aust. Ecol. 35 (1), 31–40.

Britos, A.H., Barchuk, A.H., 2008. Cambios en la cobertura y en el uso de la tierra en dos sitios del Chaco Árido del noroeste de Córdoba, Argentina. Agriscientia 25 (2), 97–110.

Brümmer, C., et al., 2008. Diurnal, seasonal, and interannual variation in carbon dioxide and energy exchange in shrub savanna in Burkina Faso (West Africa). J. Geophys. Res.: Biogeosci. 113, G02030. http://dx.doi.org/10.1029/2007JG000583.

Buchmann, N., Schulze, E.D., 1999. Net CO_2 and H_20 fluxes of terrestrial ecosystems. Global Biogeochem. Cycl. 13 (3), 751–760.

Cabrera, A.L., 1976. Regiones fitogeográficas argentinas. Enciclopedia Argentina De Agricultura Y Jardinería, 2. ACME, Buenos Aires 85 pp.

Cai, W., Cowan, T., 2012. Southeast Australia autumn rainfall reduction: a climate-Change-Induced poleward shift of ocean-atmosphere circulation. J. Clim. 26 (1), 189–205.

Contreras, S., Jobbágy, E.G., Villagra, P.E., Nosetto, M.D., Puigdefábregas, J., 2011. Remote sensing estimates of supplementary water consumption by arid ecosystems of central Argentina. J. Hydrol. 397 (1–2), 10–22.

Contreras, S., Santoni, C.S., Jobbágy, E.G., 2013. Abrupt watercourse formation in a semiarid sedimentary landscape of central Argentina: the roles of forest clearing, rainfall variability and seismic activity. Ecohydrology 6 (5), 794–805.

Falge, E., et al., 2002. Phase and amplitude of ecosystem carbon release and uptake potentials as derived from FLUXNET measurements. Agric. For. Meteorol. 113 (1–4), 75–95.

Ferrero, M.E., et al., 2013. Tree-growth responses across environmental gradients in subtropical Argentinean forests. Plant Ecol. 214 (11), 1321–1334.

Fischer, M.A., Di Bella, C.M., Jobbágy, E.G., 2012. Fire patterns in central semiarid Argentina. J. Arid Environ. 78 (0), 161–168.

Foken, T., et al., 2004. Post-field data quality control. In: Lee, X., Massman, W.J., Law, B. (Eds.), Handbook of Micrometeorology: A Guide for Surface Flux Measurement and Analysis. Kluwer Academic Publishers, Dordrecht, pp. pp. 181–208.

George, R.J., McFarlane, D.J., Nulsen, R.A., 1997. Salinity threatens the viability of agriculture and ecosystems in Western Australia. Hydrogeol. J. 5, 6–21.

Gimenez, R., Nosetto, M.D., Mercau, J.L., Paez, R., Jobbágy, E.G., 2016. The ecohydrological imprint of deforestation in the semi-arid Chaco: insights from the last forest relicts of a highly cultivated landscape. Hydrol. Process. 30, 2603–2616.

Golluscio, R.A., Escalada, V.S., Pérez, J., 2009. Minimal plant responsiveness to summer water pulses: ecophysiological constraints of three species of semiarid patagonia. Rangeland Ecol. Manag. 62 (2), 171–178.

Grossman, R., Reinsch, T., 2002. Bulk density and linear extensibility. In: Dane, J.H., Topp, G.C. (Eds.), Methods of Soil Analysis: Part 4 Physical Methods, pp. pp. 201–228.

Grünzweig, J.M., Lin, T., Rotenberg, E., Schwartz, A., Yakir, D., 2003. Carbon sequestration in arid-land forest. Global Change Biol. 9, 791–799.

Hansen, M.C., et al., 2013. High-resolution global maps of 21st-century forest cover change. Science 342 (6160), 850–853.

Hastings, S.J., Oechel, W.C., Muhlia-Melo, A., 2005. Diurnal, seasonal and annual variation in the net ecosystem CO2 exchange of a desert shrub community (Sarcocaulescent) in Baja California, Mexico. Global Change Biol. 11 (6), 927–939.

Hillel, D., 1998. Environmental Soil Physics. Academic Press, San Diego 771 pp.

Hoekstra, J.M., Boucher, T.M., Ricketts, T.H., Roberts, C., 2005. Confronting a biome crisis: global disparities of habitat loss and protection. Ecol. Lett. 8, 23–29.

Houspanossian, J., Giménez, R., Baldi, G., Nosetto, M., 2016. Is aridity restricting deforestation and land uses in the South American Dry Chaco? J. Land Use Sci. 11 (4), 369–383.

Huxman, T.E., et al., 2004. Precipitation pulses and carbon fluxes in semiarid and arid ecosystems. Oecologia 141 (2), 254–268.

Iriondo, M., 1993. Geomorphology and late quaternary of the Chaco (South America). Geomorphology 7, 289–303.

Jayawickreme, D.H., Santoni, C., Kim, J.H., Jobbágy, E.G., Jackson, R.B., 2011. Changes in hydrology and salinity accompanying a century of agricultural conversion in Argentina. Ecol. Appl. 21 (7), 2367–2379.

Jenerette, G.D., Scott, R.L., Huxman, T.E., 2008. Whole ecosystem metabolic pulses following precipitation events. Funct. Ecol. 22 (5), 924–930.

Jia, X., et al., 2016. Energy partitioning over a semi-arid shrubland in northern China. Hydrol. Processes 30 (6), 972–985.

Jobbágy, E.G., Nosetto, M.D., Santoni, C., Baldi, G., 2008. El desafío ecohidrológico de las transiciones entre sistemas leñosos y herbáceos en la llanura Chaco-Pampeana. Ecol. Austral. 18, 305–322.

Kljun, N., Calanca, P., Rotach, M.W., Schmid, H.P., 2004. A simple parameterization for flux footprint predictions. Boundary-Layer Meteorol. 112, 503–523.

Köstner, B., 2001. Evaporation and transpiration from forests in Central Europe-relevance of patch-level studies for spatial scaling. Meteorol. Atmos. Phys. 76, 69–82.

Kurc, S.A., Small, E.E., 2007. Soil moisture variations and ecosystem-scale fluxes of water and carbon in semiarid grassland and shrubland. Water Resour. Res. 43, W06416. http://dx.doi.org/10.1029/2006WR005011.

Le Houerou, H.N., Bingham, R.L., Skerbek, W., 1988. Relationship between the variability of primary production and the variability of annual precipitation in world arid lands. J. Arid Environ. 15 (1), 1–18.

Leduc, C., Favreau, G., Schroeter, P., 2001. Long-term rise in a sahelian water-table: the continental terminal in south-west Niger. J. Hydrol. 243 (1-2), 43–54.

Ludwig, J.A., Wilcox, B.P., Breshears, D.D., Tongway, D.J., Imeson, A.C., 2005. Vegetation patches and runoff-erosion as interacting ecohydrological processes in semiarid landscapes. Ecology 86 (2), 288–297.

Luo, H., et al., 2007. Mature semiarid chaparral ecosystems can be a significant sink for atmospheric carbon dioxide. Global Change Biol. 13 (2), 386–396.

Magliano, P.N., Breshears, D.D., Fernández, R.J., Jobbágy, E.G., 2015a. Rainfall intensity switches ecohydrological runoff/runon redistribution patterns in dryland vegetation patches. Ecol. Appl. 25 (8), 2094–2100.

Magliano, P.N., Fernández, R.J., Mercau, J.L., Jobbágy, E.G., 2015b. Precipitation event distribution in Central Argentina: spatial and temporal patterns. Ecohydrology 8 (1), 94–104.

Magliano, P.N., et al., 2015c. Rainwater harvesting in dry Chaco: regional distribution and local water balance. J. Arid Environ. 123, 93–102.

Magliano, P.N., et al., 2016. Cambios en la partición de flujos de agua en el Chaco Árido al reemplazar bosques por pasturas. Ecol. Austral. 26, 95–106.

Magliano, P.N., Fernández, R., Florio, E.L., Murray, F., Jobbágy, E.G., 2017a. Soil physical changes after conversion of Woodlands to pastures in dry chaco rangelands (Argentina). Rangeland Ecol. Manage. 70, 225–229.

Magliano, P.N., et al., 2017b. Litter is more effective than forest canopy reducing soil evaporation in dry Chaco rangelands. Ecohydrology e1879. http://dx.doi.org/10.1002/eco.1879.

Marchesini, V., Fernández, R.J., Jobbágy, E.G., 2013. Salt leaching leads to drier soils in disturbed semiarid woodlands of central Argentina. Oecologia 171 (4), 1003–1012.

Marchesini, V.A., 2011. Cambios en el uso de la tierra y el balance de agua en ecosistemas semiáridos: el desmonte selectivo en el Chaco árido analizado a diferentes escalas espaciales. Universidad de Buenos Aires, Buenos Aires.

Marchesini, V.A., Gimenez, R., Nosetto, M.D., Jobbágy, E.G., 2016. The ecohydrological transformation of Chaco dry forests and the risk of dryland salinity: are we following Australia's footsteps? Ecohydrology e1822. http://dx.doi.org/10.1002/eco.1822.

New, M., Lister, D., Hulme, M., Makin, I., 2002. A high-resolution data set of surface climate over global land areas. Climate Res. 21, 1–25.

Ogle, K., Reynolds, J.F., 2004. Plant responses to precipitation in desert ecosystems: integrating functional types, pulses, thresholds, and delays. Oecologia 141 (2), 282–294.

Olson, D.M., et al., 2001. Terrestrial Ecoregions of the World: a new map of life on earth: a new global map of terrestrial ecoregions provides an innovative tool for conserving biodiversity. Bioscience 51 (11), 933–938.

Peña Zubiate, C.A., Anderson, D.L., Demmi, M.A., Saenz, J.L., D'Hiriart, A. (Eds.), 1998. Carta De Suelos Y Vegetación De La Provincia De San Luis. Instituto Nacional de Tecnología Agropecuaria (INTA), San Luis, Argentina.

Perez-Ruiz, E.R., et al., 2010. Carbon dioxide and water vapour exchange in a tropical dry forest as influenced by the North American monsoon System (NAMS). J. Arid Environ. 74 (5), 556–563.

Posse, G., et al., 2014. Attribution of carbon dioxide fluxes to crop types in a heterogeneous agricultural landscape of Argentina. Environ. Model. Assess. 19 (5), 361–372.

Poulter, B., et al., 2014. Contribution of semi-arid ecosystems to interannual variability of the global carbon cycle. Nature 509 (7502), 600–603.

Raz-Yaseef, N.R., Yakir, D., Rotenberg, E., Schiller, G., Cohen, S., 2010. Ecohydrology of a semi-arid forest: partitioning among water balance components and its implications for predicted precipitation changes. Ecohydrology 3, 143–154.

Reichstein, M., et al., 2005. On the separation of net ecosystem exchange into assimilation and ecosystem respiration: review and improved algorithm. Global Change Biol. 11

(9), 1424–1439.
Reichstein, M., et al., 2002. Severe drought effects on ecosystem CO2 and H2O fluxes at three Mediterranean evergreen sites: revision of current hypotheses? Global Change Biol. 8 (10), 999–1017.
Rich, P.M., Wood, J., Vieglais, D.A., Burek, K., Webb, N., 1999. Guide to Hemiview: Software for Analysis of Hemispherical Photography. Cambridge University Press.
Rotenberg, E., Yakir, D., 2010. Contribution of semi-arid forests to the climate system. Science 327, 451–454.
Running, S.W., et al., 1999. A global terrestrial monitoring network integrating tower fluxes, flask sampling, ecosystem modeling and EOS satellite data. Remote Sens. Environ. 70 (1), 108–127.
Sala, O.E., Gherardi, L.A., Reichmann, L., Jobbágy, E., Peters, D., 2012. Legacies of precipitation fluctuations on primary production: theory and data synthesis. Phil. Trans. R. Soc. B : Biol. Sci. 367 (1606), 3135–3144.
Sala, O.E., Lauenroth, W.K., 1982. Small rainfall events: an ecological role in semiarid regions. Oecologia 53 (3), 301–304.
Salvucci, M.E., Crafts-Brandner, S.J., 2004. Relationship between the heat tolerance of photosynthesis and the thermal stability of rubisco activase in plants from contrasting thermal environments. Plant Physiol. 134 (4), 1460–1470.
Santoni, C.S., Jobbágy, E.G., Contreras, S., 2010. Vadose transport of water and chloride in dry forests of central Argentina: the role of land use and soil texture. Water Resour. Res. 46 (10), W10541.
Saulo, C., Ruiz, J., Skabar, Y.G., 2007. Synergism between the low-level jet and organized convection at its exit region. Monthly Weather Rev. 135 (4), 1310–1326.
Scanlon, B.R., Reedy, R.C., Stonestrom, D.A., Prudic, D.E., Dennehy, K.F., 2005. Impact of land use and land cover change on groundwater recharge and quality in the southwestern US. Global Change Biol. 11 (10), 1577–1593.
Scott, R.L., Huxman, T.E., Williams, D.G., Goodrich, D.C., 2006. Ecohydrological impacts of woody-plant encroachment: seasonal patterns of water and carbon dioxide exchange within a semiarid riparian environment. Global Change Biol. 12 (2), 311–324.
Scott, R.L., Jenerette, G.D., Potts, D.L., Huxman, T.E., 2009. Effects of seasonal drought on net carbon dioxide exchange from a woody-plant-encroached semiarid grassland. J. Geophys. Res. 114, G04004. http://dx.doi.org/10.1029/2008JG000900.
Schwinning, S., Sala, O.E., 2004. Hierarchy of responses to resource pulses in arid and semi-arid ecosystems. Oecologia 141 (2), 211–220.
Seyfried, M.S., et al., 2005. Ecohidrological control of deep drainage in arid and semiarid regions. Ecology 86 (2), 277–287.
Sims, D.A., et al., 2006. On the use of MODIS EVI to assess gross primary productivity of North American ecosystems. J. Geophys. Res. 111, G4. http://dx.doi.org/10.1029/2006JG000162. G04015.
Smith, S.D., et al., 2000. Elevated CO2 increases productivity and invasive species success in an arid ecosystem. Nature 408 (6808), 79–82.
Stannard, D.I., Weltz, M.A., 2006. Partitioning evapotranspiration in sparsely vegetated rangeland using a portable chamber. Water Resour. Res. 42, W02413. http://dx.doi.org/10.1029/2005WR004251.
Steinaker, D.F., et al., 2016. Vegetation composition and structure changes following roller-chopping deforestation in central Argentina woodlands. J. Arid Environ. 133, 19–24.
Toby Pennington, R., Prado, D.E., Pendry, C.A., 2000. Neotropical seasonally dry forests and Quaternary vegetation changes. J. Biogeogr. 27 (2), 261–273.
Tripaldi, A., et al., 2013. Geological evidence for a drought episode in the western Pampas (Argentina, South America) during the early-mid 20th century. Holocene 23 (12), 1731–1746.
Vallejos, M., et al., 2015. Transformation dynamics of the natural cover in the Dry Chaco ecoregion: a plot level geo-database from 1976 to 2012. J. Arid Environ. 123, 3–11.
Verduzco, V.S., et al., 2015. Variations of net ecosystem production due to seasonal precipitation differences in a tropical dry forest of northwest Mexico. J. Geophys. Res.: Biogeosci. 120 (10), 2081–2094.
Webb, E.K., Pearman, G.I., Leuning, R., 1980. Correction of flux measurements for density effects due to heat and water vapour transfer. Q. J. R. Meteorol. Soc. 106 (447), 85–100.
Wilczak, J.M., Oncley, S.P., Stage, S.A., 2001. Sonic anemometer tilt correction algorithms. Boundary-Layer Meteorol. 99 (1), 127–150.
Wilson, G.V., Luxmore, R.J., 1988. Infiltration, macroporosity, and mesoporosity distributions on two forest watersheds. Soil Sci. Soc. Am. J. 52, 329–335.
Wilson, K.B., Baldocchi, D.D., 2000. Seasonal and interannual variability of energy fluxes over a broadleaved temperate deciduous forest in North America. Agric. For. Meteorol. 100 (1), 1–18.
Wilson, K.B., et al., 2002. Energy balance closure at FLUXNET sites. Agric. For. Meteorol. 113, 223–243.
Wofsy, S.C., et al., 1993. Net exchange of CO2 in a mid-latitude forest. Science 260 (5112), 1314.
Yahdjian, L., Sala, O.E., 2006. Vegetation structure constrains primary production response to water availability in the patagonian steppe. Ecology 87 (4), 952–962.
Zak, M., Cabido, M., Cáceres, D., Díaz, S., 2008. What drives accelerated land cover change in central Argentina? synergistic consequences of climatic, socioeconomic, and technological factors. Environ. Manage. 42 (2), 181–189.
Zhao, J., Hartmann, H., Trumbore, S., Ziegler, W., Zhang, Y., 2013. High temperature causes negative whole-plant carbon balance under mild drought. New Phytol. 200 (2), 330–339.